Study on Optical Properties of Rare-Earth Ions in Nanocrystalline Monoclinic $SrAl_2O_4$: Ln (Ln = Ce^{3+}, Pr^{3+}, Tb^{3+})

Zuoling Fu, Shihong Zhou, and Siyuan Zhang*

Laboratory of Rare Earth Chemistry and Physics, Changchun Institute of Applied Chemistry, Graduate School of the Chinese Academy Sciences, Changchun 130022, China

Received: March 14, 2005; In Final Form: May 11, 2005

$SrAl_2O_4$: Ln (Ln = Ce^{3+}, Pr^{3+}, Tb^{3+}) nanocrystals have been synthesized by the combustion method. The results of XRD indicated that the resulting $SrAl_2O_4$: Ln (Ln = Ce^{3+}, Pr^{3+}, Tb^{3+}) nanocrystals have a reduced and distorted monoclinic lattice compared with bulk materials. The spectral properties are measured, and it is found that the excitation peaks of 5d energy levels red shift in nanocrystals in contrast to that in bulk crystals. The mechanism of spectra and energy changes is investigated. The order of the degree of red shift for nano $SrAl_2O_4$: Ln (Ln = Ce^{3+}, Pr^{3+}, Tb^{3+}) crystals is $Pr^{3+} > Ce^{3+} > Tb^{3+}$, which is in good agreement with our predicted results.

1. Introduction

The fluorescence of Ce^{3+}-activated compounds is well known.[1] Usually the emission consists of a broad band with two peaks in the long-wavelength ultraviolet region, which is due to a 5d−4f transition. Other trivalent lanthanide ions such as Pr^{3+} and Tb^{3+} also have fluorescence from $4f^{N-1}5d$ to $4f^N$-configurations in the near-ultraviolet (UV) or UV spectral domain. The understanding of optical properties of Ce^{3+}, Pr^{3+}, and Tb^{3+} in inorganic compounds is of great importance due to the potential technological applications as functional photonic materials such as optical fiber amplifiers, lasers, and wavelength converting devices.[2−4]

Strontium aluminate ($SrAl_2O_4$) has been proven to be an efficient host material with a wide band gap, which offers the possibility of generating broad band emissions.[5] We have investigated the photoluminescence of Eu^{2+} doped in the bulk and nano $SrAl_2O_4$ crystals.[6] $SrAl_2O_4$ has an enclosed and stiff structure like SrB_4O_7.[7,8] The monoclinic structure is constructed by corner-sheared AlO_4 tetrahedrons forming zigzag strings, and Sr ions penetrate to the opening of the structure. The tetrahedronal anion group (AlO_4) is helpful to the existence of the deoxidized ions (Eu^{2+}, Ce^{3+}, Pr^{3+}, Tb^{3+}). Therefore, we synthesized the bulk and nano $SrAl_2O_4$: Ln (Ln = Ce^{3+}, Pr^{3+}, Tb^{3+}) crystals by the solid-state method and combustion method, respectively. We were interested to study the differences on the optical properties of Ce^{3+}, Pr^{3+}, and Tb^{3+} in the same host materials with different forms. Furthermore, we focused on investigating the mechanism of spectral and energy changes.

2. Experimental Section

The bulk $SrAl_2O_4$: Ln (Ln = Ce^{3+}, Pr^{3+}, Tb^{3+}) crystals were obtained using a high-temperature solid-state reaction technique. The reactants include analytical grade pure $SrCO_3$ and Al_2O_3 and 99.99% pure rare-earth oxides CeO_2, Tb_4O_7, and Pr_2O_3. According to the nominal compositions of compounds $Sr_{0.99}Ln_{0.01}Al_2O_4$ (Ln = Ce^{3+}, Pr^{3+}, Tb^{3+}), appropriate amounts of starting materials were thoroughly mixed and ground then heated at 700 °C for 2 h. After being reground, they were calcined at 1400 °C for 5 h in a thermal-carbon reducing atmosphere. Nano $SrAl_2O_4$: Ln (Ln = Ce^{3+}, Pr^{3+}, Tb^{3+}) crystals were prepared by combustion synthesis method. Starting materials were $Sr(NO_3)_2$ (0.2 M), $Al(NO_3)_3$ (0.2 M), $Ln(NO_3)_3$(Ln = Ce^{3+}, Pr^{3+}, Tb^{3+}) (0.1 M), and urea (0.2 M) solutions. Appropriate volumes were mixed in an evaporating dish and the molar ratio of urea to NO_3^- was 1:1.5. Adjusting the ratio can control the size of the grain. After full stirring, the precursor solution was introduced into a muffle furnace maintained at 600 °C with a lid. Initially, the solution boiled and underwent dehydration, followed by decomposition with the evolution of large amounts of gases (oxides of carbon, nitrogen, and ammonia). Then, spontaneous combustion with enormous swelling produced foamy and voluminous $SrAl_2O_4$:Ce^{3+}, $SrAl_2O_4$:Pr^{3+}, and $SrAl_2O_4$:Tb^{3+}. The whole process is over within less than 5 min. In addition, it should be mentioned that the activator (Ce^{3+}, Pr^{3+}, Tb^{3+}) content was maintained at 1 mol % for all the prepared samples.

The X-ray powder diffraction pattern was measured with a Rigaku D/max-IIB X-ray diffractometer, using CuK_α (λ = 1.5405 Å) radiation. The average crystallite sizes of the $SrAl_2O_4$: Ln (Ln = Ce^{3+}, Pr^{3+}, Tb^{3+}) nanocrystalline can be estimated by the Debye−Scherrer equation: $D = K\lambda/\beta \cos\theta$, where D is the average diameter of the particles, K is the Scherrer constant equal to 0.89, λ is the wavelength of the CuK_α-radiation, β is the corrected full width at half-maximum (FWHM), and θ is the Bragg angle. The calculated crystallite size for $SrAl_2O_4$:Ce^{3+}, $SrAl_2O_4$:Pr^{3+}, and $SrAl_2O_4$:Tb^{3+} were 28, 23, and 19 nm at room temperature, respectively. In addition, the refined crystallographic unit cell parameters were obtained and listed in Table 1. The values of all samples are roughly matched with $SrAl_2O_4$ standard values given in the Joint Committee of Powder Diffraction (JCPDS No. 34-379). A decreasing trend of unit cell parameter values in nanocrystals could clearly be observed compared with the bulk materials. Photoluminescence measurements were performed on a Hitachi F-4500 fluorescence spectrophotometer at room temperature. It should be mentioned that the photoluminescence measure-

* Corresponding author. E-mail: syzhang@ciac.jl.cn; Fax: 86-431-5698041.

10.1021/jp051313p CCC: $30.25
Published on Web 07/13/2005

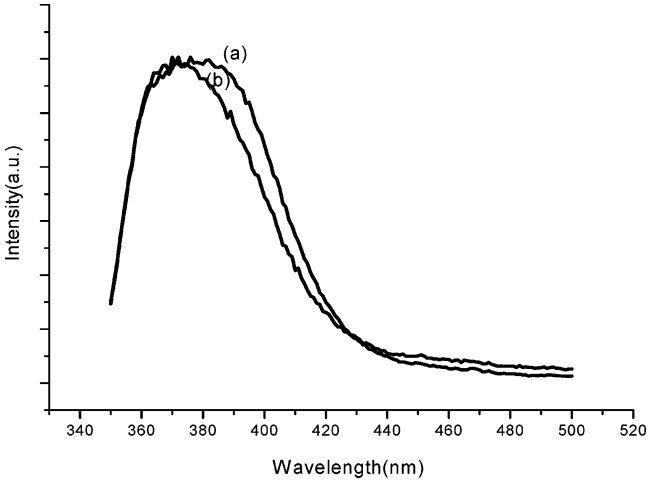

Figure 1. Emission spectra for (a) bulk $SrAl_2O_4$: Ce^{3+} crystal at λ_{ex} = 328 nm, (b) nano $SrAl_2O_4$: Ce^{3+} crystal at λ_{ex} = 332 nm at room temperature.

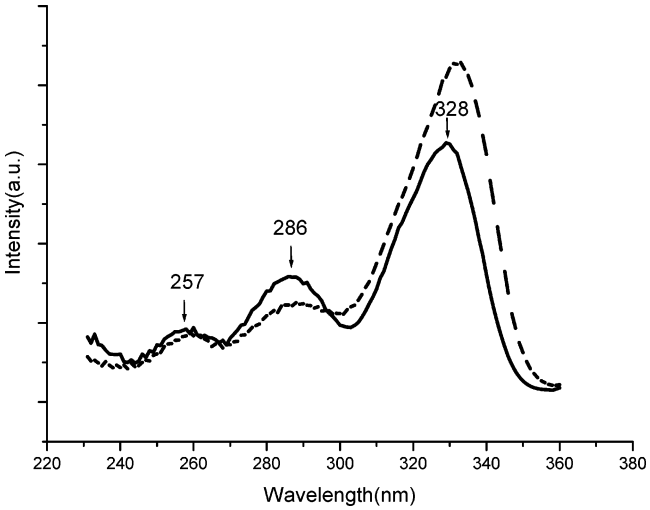

Figure 2. Excitation spectra of bulk $SrAl_2O_4$: Ce^{3+} crystal (solid line) and nano $SrAl_2O_4$: Ce^{3+} crystal (dot line) at room temperature (λ_{em} = 380 nm).

ments were performed under the same conditions for the like-kind samples.

3. Results and Discussion

3.1. Photoluminescence and Excitation Spectra. Emission and excitation spectra of Ce^{3+} in the bulk and nano $SrAl_2O_4$ crystals are shown in Figures 1 and 2, respectively. The emission of Ce^{3+} usually includes two bands of the transitions of the 5d excited state to $^2F_{7/2}$ and $^2F_{5/2}$ states. The emission spectrum observed in bulk $SrAl_2O_4$: Ce^{3+} crystals seems to consist of two of them in a single band, peaking at 380 nm (at 371 nm in nano $SrAl_2O_4$: Ce^{3+} crystals). Its excitation peaks are found at 257, 286, and 328 nm (30488 cm^{-1}) in Figure 2, which correspond to the transitions from the ground state of Ce^{3+} to its crystal field splitting levels of $5d^1$ states.[9] While in nano $SrAl_2O_4$: Ce^{3+} crystals there are also three similar broad bands peaking at about 259, 287, and 332 nm (30120 cm^{-1}). It is obvious that the position of the excitation band in nanocrystals shifts to lower energies compared with the bulk materials.

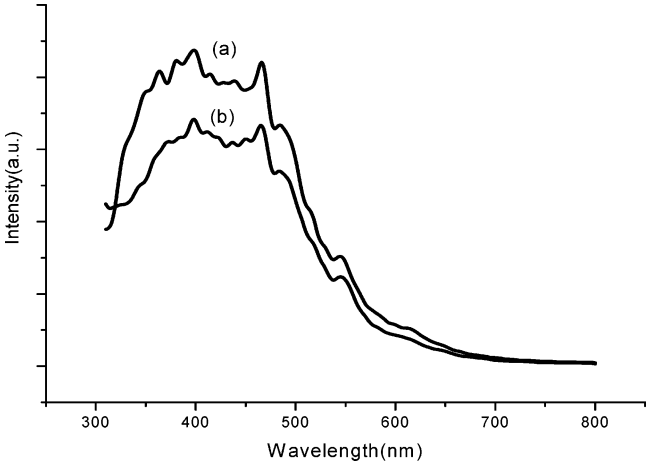

Figure 3. Emission spectra for (a) bulk $SrAl_2O_4$: Pr^{3+} crystal at λ_{ex} = 236 nm, (b) nano $SrAl_2O_4$: Pr^{3+} crystal at λ_{ex} = 239 nm at room temperature.

In Figure 3 the emission spectra of Pr^{3+} in bulk and nano $SrAl_2O_4$ crystals are plotted. The broad peak in the range of 310−650 nm is assigned to the 5d−4f energy level transition. The sharp peaks located at the broad band come from f−f transitions of Pr^{3+}. Figure 4 displays the excitation spectra of $SrAl_2O_4$: Pr^{3+}. In bulk $SrAl_2O_4$: Pr^{3+} crystal, the dominant band with a maximum at 236 nm (42373 cm^{-1}) is assignable to be the lowest $4f^2 \rightarrow 4f^15d^1$ transition for Pr^{3+} in the host lattice. Compared with the bulk materials, there was an obvious broad peak at 239 nm (41841 cm^{-1}) in nano $SrAl_2O_4$: Pr^{3+} crystal, which indicated that the lowest excited band in nanocrystal shifted to the longer wavelength.

The emission spectra of Tb^{3+} in bulk and nano $SrAl_2O_4$ are shown in Figure 5. The Tb^{3+} emission peaks are found at 380, 414, 436, 458, and 470 nm, which are assigned to the $^5D_3$ to ^7F_J (J = 6, 5, 4, 3, 2) transitions. Other emission peaks from $^5D_4$ to ^7F_J (J = 6, 5, 4, 3) are also found at 487, 540, 583, and 621 nm, respectively. The excitation spectra of Tb^{3+} in bulk $SrAl_2O_4$ are shown in Figure 6. The excitation peaks are found to be strong at 232 nm and another weaker peak at higher energies. The strong 232 nm (43103 cm^{-1}) peak is related to the f−d excitation of the Tb^{3+}, and the other peak may be the higher excited-state level transition. From Figure 6, it is also seen that the lowest 5d level excitation band in nano $SrAl_2O_4$: Tb^{3+} has slightly red-shifted in contrast to that of the bulk materials, and is situated at 233 nm (42918 cm^{-1}).

As demonstrated by Dorenbos in an extensive review on the position of 5d transitions of lanthanides, it is possible to use the position of 5d levels of Ce^{3+} to predict that of all other lanthanides.[10,11] This is true for Ce^{3+}, Pr^{3+}, and Tb^{3+} in $SrAl_2O_4$.

TABLE 1: Unit Cell Parameters for $Sr_{1-x}Al_2O_4$: Ln_x (x = 0.01, Ln = Ce^{3+}, Pr^{3+}, Tb^{3+}) Bulk and Nanocrystalline Samples

sample	a (Å)	b (Å)	c (Å)	β (°)
JCPDS std no. 34-379	8.447	8.816	5.163	93.42
$SrAl_2O_4$: Ce^{3+} (bulk)	8.431 ± 0.0007	8.816 ± 0.0069	5.155 ± 0.0125	93.41 ± 0.0014
$SrAl_2O_4$: Ce^{3+} (nano)	8.421 ± 0.0006	8.807 ± 0.0054	5.159 ± 0.0030	93.36 ± 0.0601
$SrAl_2O_4$: Pr^{3+} (bulk)	8.432 ± 0.0009	8.817 ± 0.0012	5.155 ± 0.0007	93.40 ± 0.0109
$SrAl_2O_4$: Pr^{3+} (nano)	8.428 ± 0.0018	8.808 ± 0.0073	5.150 ± 0.0019	93.38 ± 0.0237
$SrAl_2O_4$: Tb^{3+} (bulk)	8.441 ± 0.0007	8.816 ± 0.0011	5.156 ± 0.0124	93.43 ± 0.0013
$SrAl_2O_4$: Tb^{3+} (nano)	8.421 ± 0.0007	8.808 ± 0.0006	5.148 ± 0.0097	93.29 ± 0.0058

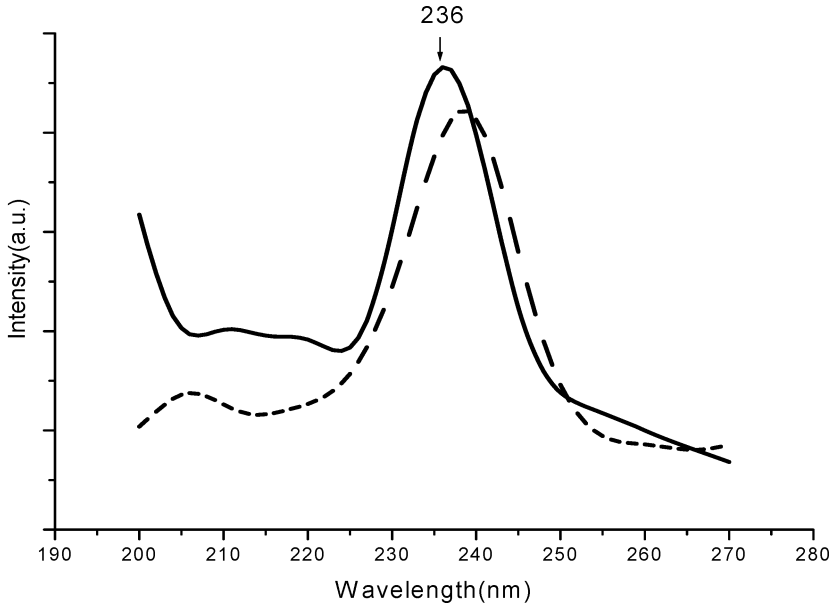

Figure 4. Excitation spectra of bulk $SrAl_2O_4$: Pr^{3+} crystal (solid line) and nano $SrAl_2O_4$: Pr^{3+} crystal (dot line) at room temperature ($\lambda_{em} = 360$ nm).

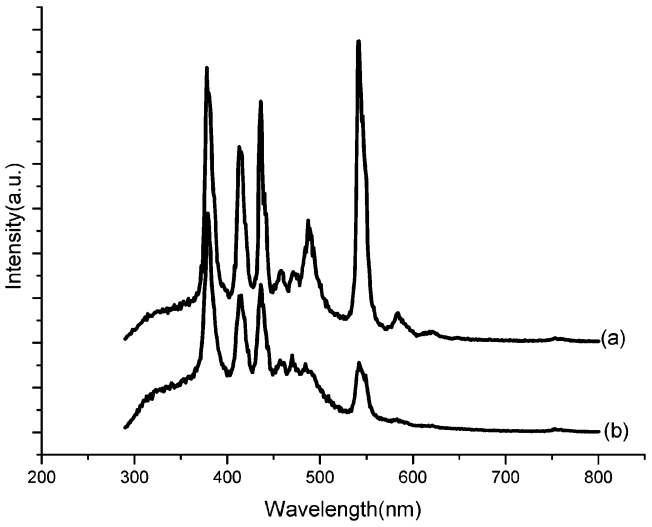

Figure 5. Emission spectra for (a) bulk $SrAl_2O_4$: Tb^{3+} crystal ($\lambda_{ex} = 232$ nm), (b) nano $SrAl_2O_4$: Tb^{3+} crystal ($\lambda_{ex} = 233$ nm).

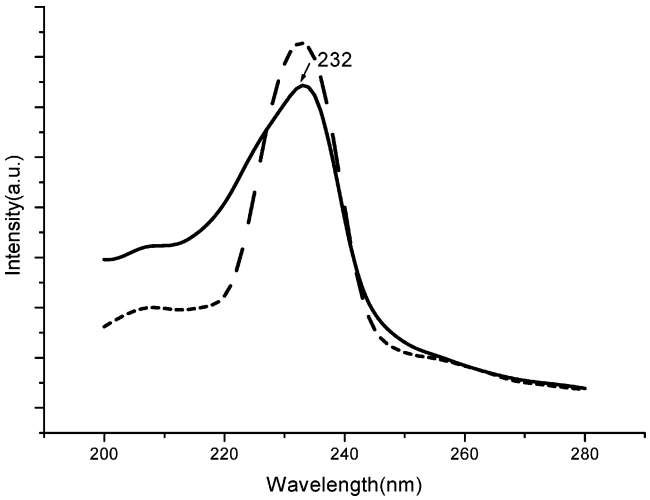

Figure 6. Excitation spectra of bulk $SrAl_2O_4$: Tb^{3+} crystal (solid line) and nano $SrAl_2O_4$: Tb^{3+} crystal (dot line) at room temperature ($\lambda_{em} = 380$ nm).

From the observed energy of the lowest 5d state for Ce^{3+} in $SrAl_2O_4$ (30487 cm^{-1}), the lowest 5d level of Pr^{3+} in this host lattice can be predicted to be about 238 nm and the lowest 5d level of Tb^{3+} in this host lattice can be predicted to be about 233 nm. These results are in line with the band we observed, which corroborates the attribution of these bands.

3.2. Spectral Analysis. As is well known, the luminescent spectra of lanthanide ions in crystals arise mainly from two types of electronic transitions: 4f−4f and 4f−5d transitions. The former generally show sharp line emission while the latter have broad band character, and the crystalline environment has a greater effect on interconfigurational transitions of Ln^{3+} than on intraconfigurational transitions within the shielded 4f. This is because the excited states such as 5d are not shielded from the surrounding electronic shell, and the 5d electron has a strong interaction with the neighboring anion ligands in the compound. In addition, the 5d energy level has closer relation to the conduction band of the compound, when the grain size becomes small, the band gap may become wide, then the 5d energy level also changes correspondingly.

The interactions for the $4f^{N-1}5d$ configuration, which may be important for optical spectrum simulations, are as follows:

$$H = H_0 + H_{\mathrm{Coul}}(\mathrm{ff}) + H_{\mathrm{so}}(\mathrm{f}) + H_{\mathrm{cf}}(\mathrm{f}) + H_{\mathrm{cf}}(\mathrm{d}) + H_{\mathrm{so}}(\mathrm{d}) + H_{\mathrm{Coul}}(\mathrm{fd})$$

where H_0 is the central-field interaction which includes the kinetic energy of electron and the Coulomb interaction between the $4f^{N-1}$ core and the electrons; the next three terms are Coulomb, spin−orbit and crystal-field interactions for the $4f^{N-1}$ core; the fifth and sixth terms are crystal-field and spin−orbit interactions for the single 5d electron; and the last term H_{Coul}(fd) is the Coulomb interaction between the $4f^{N-1}$ core and the 5d electron. Not all the interactions are of the same importance. The order of magnitude of the energy splitting caused by these interactions is $H_0 > [H_{\mathrm{Coul}}(\mathrm{ff}), H_{\mathrm{cf}}(\mathrm{d})] > H_{\mathrm{Coul}}(\mathrm{fd}) > H_{\mathrm{so}}(\mathrm{f}) > H_{\mathrm{so}}(\mathrm{d}) > H_{\mathrm{cf}}(\mathrm{f})$. The interactions $H_{\mathrm{so}}(\mathrm{d})$ and $H_{\mathrm{cf}}(\mathrm{f})$ can be generally ignored. Therefore, $H = H_0 + H_{\mathrm{Coul}}(\mathrm{ff}) + H_{\mathrm{Coul}}(\mathrm{fd}) + H_{\mathrm{cf}}(\mathrm{d}) + H_{\mathrm{so}}(\mathrm{f})$ would be most suitable for constructing the bases of the $4f^{N-1}5d$ configuration. In our case, it is expected that $H_{\mathrm{Coul}}(\mathrm{ff})$ and $H_{\mathrm{so}}(\mathrm{f})$ are unchanged in bulk and nanocrystals.

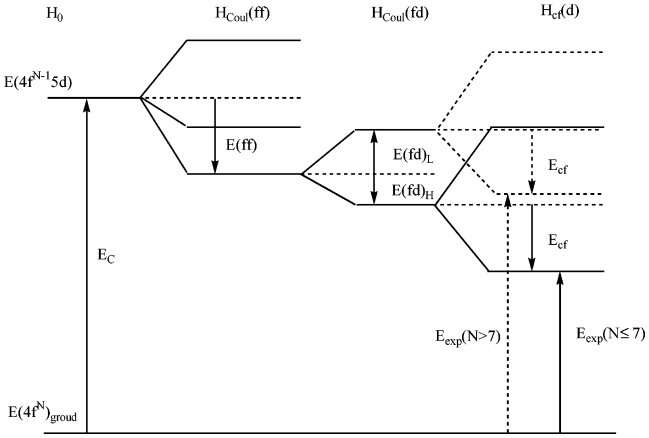

Figure 7. A schematic energy diagram of the $4f^{N-1}5d$ configuration of Ln^{3+} in any crystal A.

TABLE 2: Values of Corresponding Crystal Factors for $Sr_{1-x}Al_2O_4$: Ln_x ($x = 0.01$, Ln = Ce^{3+}, Pr^{3+}, Tb^{3+}) Bulk and Nanocrystalline Samples

sample	d (Å)	h_e	F_c
$SrAl_2O_4$: Ce^{3+} (bulk)	2.7665	0.5508	0.3782
$SrAl_2O_4$: Ce^{3+} (nano)	2.7650	0.5500	0.3787
$SrAl_2O_4$: Pr^{3+} (bulk)	2.7667	0.5509	0.3781
$SrAl_2O_4$: Pr^{3+} (nano)	2.7645	0.5500	0.3789
$SrAl_2O_4$: Tb^{3+} (bulk)	2.7678	0.5514	0.3778
$SrAl_2O_4$: Tb^{3+} (nano)	2.7633	0.5513	0.3792

Figure 7 shows a schematic energy diagram of the $4f^{N-1}5d$ configuration of Ln^{3+} in any crystal A. It is shown that the energy level change results from three interactions for Ln^{3+}, the shift of the energy centroid (E_c) of the 5d orbital, the Coulomb interactions between 4f and 4f electrons (E_{Coul}(ff)) and between 4f and 5d electrons (E_{Coul}(fd)), and the effect of the crystal field (E_{cf}(d)). For the light lanthanide ions of $N \leq 7$(N is the electron number of the 4f orbital), the energy level position of the spin-allowed transition is lower than that of the spin-forbidden transition. While the energy level position of the spin-allowed transition is higher than that of the spin-forbidden transition when $N > 7$. We assume that E_{exp} denotes the lowest energy level of a 5d state in the experimental spectra of a crystal, then, for the light lanthanide ions of $N \leq 7$, the following equation can be obtained from the energy diagram:

$$E^b_{exp} = E^b_c - E^b_{Coul}(ff) - E^b_{Coul}(fd)_H - E^b_{cf}(d)$$

Also, for the heavy lanthanide ions of $N > 7$,

$$E^b_{exp} = E^b_c - E^b_{Coul}(ff) + E^b_{Coul}(fd)_L - E^b_{cf}(d)$$

where b indicates the parameter values in bulk crystals. The subscript indices (H and L) describe the high spin state and the low spin state from interaction between f and d electrons, respectively. According to refs 12−14, E_c, E_{Coul}(ff), and E_{Coul}(fd) are related to the environmental factor h_e and E_{cf}(d) is concerned with the environmental parameter F_c. Both h_e and F_c are the factors depending on the crystals. When the particle size becomes small, the unit cell volume accordingly becomes small. The calculated results of h_e and F_c are listed in Table 2. One can notice that h_e of the nanocrystal has a decreasing trend compared with the bulk counterpart. A decrease of h_e leads to an increase of E_c, which indicates that the central energy E_c in nanocrystals has an ascending trend; E_{Coul}(ff) and E_{Coul}(fd) also increase. At the same time, the bond length Sr−O becomes shorter in nanocrystals (see d value in Table 2), which results in an increase of the crystal field strength around the rare earth ions, Consequently, E_{cf}(d) will increase in nanocrystals. Finally, in nanocrystals, we can obtain

$$E^n_c = E^b_c + \delta E_c$$

$$E^n_{Coul}(fd)_H = E^b_{Coul}(fd)_H + \delta E_{Coul}(fd)_H$$

$$E^n_{Coul}(fd)_L = E^b_{Coul}(fd)_L + \delta E_{Coul}(fd)_L$$

$$E^n_{cf}(d) = E^b_{cf}(d) + \delta E_{cf}(d)$$

Then, for $N \leq 7$:

$$E^n_{exp} = E^b_c + \delta E_c - E^n_{Coul}(ff) - E^b_{Coul}(fd)_H - \delta E_{Coul}(fd)_H - E^b_{cf}(d) - \delta E_{cf}(d)$$

and for $N > 7$:

$$E^n_{exp} = E^b_c + \delta E_c - E^n_{Coul}(ff) + E^b_{Coul}(fd)_L + \delta E_{Coul}(fd)_L - E^b_{cf}(d) - \delta E_{cf}(d)$$

where the footnote with n indicates the parameter values in nanocrystals and δ denotes increment in nanocrystals. Since the 4f electron is less influenced by crystal environment, it is considered $E^n_{Coul}(ff) = E^b_{Coul}(ff)$ and then we can obtain

$$\Delta E = E^n_{exp} - E^b_{exp} = \delta E_c - \delta E_{Coul}(fd)_H - \delta E_{cf}(d)\ (N \leq 7)$$

$$\Delta E = E^n_{exp} - E^b_{exp} = \delta E_c + \delta E_{Coul}(fd)_L - \delta E_{cf}(d)\ (N > 7)$$

The spectra of Ce^{3+} are simpler than that of the other Ln^{3+}, because the Ce^{3+} ion only has one electron in the 4f orbital, and irradiation will excite this 4f electron into a 5d orbital, leaving the 4f shell empty; consequently, the excitation spectrum of Ce^{3+} will give direct information on the crystal-field splitting and central energy of 5d orbitals. For the $4f^2 \rightarrow 4f^1 5d^1$ transition of Pr^{3+} and the $4f^8 \rightarrow 4f^7 5d^1$ transition of Tb^{3+}, their spectra are more complex compared with that of Ce^{3+}, because the $4f^{N-1}5d$ configurations of Pr^{3+} and Tb^{3+} contain the Coulomb interaction between d and f electrons, except the crystal-field splitting and descend of central energy. Therefore, when the luminescent mechanism of Ce^{3+} in any compound A is known, the luminescent behaviors of other trivalent lanthanide ions in the same host can be predicted through above-mentioned physical analysis.

3.3. Application to the $4f^N \rightarrow 4f^{N-1}5d$ Transitions of Pr^{3+} and Tb^{3+} in Bulk and Nano $SrAl_2O_4$ Crystals. The excitation spectra for $SrAl_2O_4$: Ln (Ln = Ce^{3+}, Pr^{3+}, Tb^{3+}) are chosen as an example for our investigation (see section 3.1). For Ce^{3+} ion, the energy change $\Delta E = \delta E_c - \delta E_{cf}(d)$ because of E_{Coul}(fd) = 0. The excitation spectra in nano $SrAl_2O_4$: Ce^{3+} crystal show apparent red shifts in comparison with that of the bulk crystal (from 328 nm to 332 nm), which indicates that the descent of energy level caused by crystal-field splitting is more than the ascent of central energy level of 5d orbitals. For Pr^{3+} ion, $\Delta E = \delta E_c - \delta E_{Coul}(fd)_H - \delta E_{cf}(d)$, therefore it can be concluded that the excitation spectra in nano $SrAl_2O_4$: Pr^{3+} crystal should show red shift in comparison with that of the bulk crystal, and the degree of the red shift is larger than that of Ce^{3+} ion due to the contribution of $\delta E_{Coul}(fd)_H$. In experimental spectra, the lowest 5d level in nano $SrAl_2O_4$: Ce^{3+} crystal shifts downward by 368 cm^{-1} (from 328 nm to 332 nm);

the lowest 5d level in nano $SrAl_2O_4$: Pr^{3+} crystal shifts downward by 532 cm^{-1} (from 236 nm to 239 nm). The experimental results are consistent with the predicted results. For Tb^{3+} ion, $\Delta E = \delta E_c + \delta E_{Coul}(fd)_L - \delta E_{cf}(d)$, because $\delta E_{Coul}(fd)_L$ makes the energy level shift upward, it can be predicted that the degree of the red shift in nano $SrAl_2O_4$: Tb^{3+} must be smaller than that of Ce^{3+}. In Figure 6, the lowest 5d level excitation band in nano $SrAl_2O_4$: Tb^{3+} has slightly red shifted about 185 cm^{-1}. Finally, it is concluded that the order of the degree of red shift for nano $SrAl_2O_4$: Ln (Ln = Ce^{3+}, Pr^{3+}, Tb^{3+}) crystals is $Pr^{3+} > Ce^{3+} > Tb^{3+}$, which is in good agreement with our experimental results. By contrast, it is found that, although the order of magnitude of the spectral change is small, the analysis reflects a profound physical mechanism and it can be applicable to the spectral prediction of other rare-earth-doped nanomaterials.

4. Conclusion

Nanocrystals $SrAl_2O_4$: Ln(Ln = Ce^{3+}, Pr^{3+}, Tb^{3+}) have been prepared by combustion synthesis. The excitation spectra of $SrAl_2O_4$: Ln(Ln = Ce^{3+}, Pr^{3+}, Tb^{3+}) nanocrystals shift to the lower energy in contrast to the bulk materials. It is predicted that the order of the degree of red shift for nano $SrAl_2O_4$: Ln (Ln = Ce^{3+}, Pr^{3+}, Tb^{3+}) crystals is $Pr^{3+} > Ce^{3+} > Tb^{3+}$, which corresponds reasonably with our experimental results. The physical reason for spectral and energy level changes is analyzed in detail to be a comprehensive result from the shift of the energy centroid of the 5d orbital, the Coulomb interaction between 4f and 5d electrons, and the crystal-field splitting of 5d energy level.

References and Notes

(1) Blasse, G.; Bril, A. *J. Chem. Phys.* **1967**, *47*, 5139−5145.
(2) Fouassier, C. *Curr. Opin. Solid State Mater. Sci.* **1997**, *2*, 231−235.
(3) Nicolast, S.; Laroche, M.; Girard, S.; Moncorge, R.; Guyot, Y.; Joubert, M. F.; Descroix, E.; Petrosyan, A. G. *J. Phys.: Condens. Matter* **1999**, *11*, 7937−7946.
(4) Laroche, M.; Bettinelli, M.; Girard, S.; Moncorge, R. *Chem. Phys. Lett.* **1999**, *311*, 167−172.
(5) Palilla, F. C.; Levine, A. K.; Tomkus, M. R. *J. Electrochem. Soc.* **1968**, *115*, 642−644.
(6) Fu, Z. L.; Zhou, S. H.; Yu, Y. N.; Zhang, S. Y. *Chem. Phys. Lett.* **2004**, *395*, 285−289.
(7) Schulze, V. A. R.; Mueller-Buschbaum, H. *Z. Anorg. Allg. Chem.* **1981**, *475*, 205−210.
(8) Perloff, A.; Block, S. *Acta Crystallogr.* **1966**, *20*, 274−278.
(9) Huttl, B.; Troppenz, U.; Velthaus, K. O.; Ronda, C. R.; Mauch, R. H. *J. Appl. Phys.* **1995**, *78*, 7282.
(10) Dorenbos, P. *J. Lumin.* **2000**, *91*, 91−106.
(11) Dorenbos, P. *Phys. Rev. B* **2000**, *62*, 15640−15649.
(12) Shi, J. S.; Zhang, S. Y. *J. Phys.: Condens. Matter* **2003**, *15*, 4101−4107.
(13) Shi, J. S.; Wu, Z. J.; Zhou, S. H.; Zhang, S. Y. *Chem. Phys. Lett.* **2003**, *380*, 245−250.
(14) Shi, J. S.; Zhang, S. Y. *J. Phys. Chem. B* **2004**, *108*, 18845−18849.